Synthesis, Crystal Structure, Electrochemistry and Electronic Paramagnetic Resonance Spectroscopy of $[M\{(PPh_2CH_2)_3CMe\}(o\text{-}S_2C_6H_4)][PF_6]_n$ (M = Fe, Co or Rh; n = 0 or 1)†

Carlo A. Ghilardi,[a] Franco Laschi,[b] Stefano Midollini,[a] Annabella Orlandini,[a] Giancarlo Scapacci[a] and Piero Zanello[b]

[a] *Istituto per lo Studio della Stereochimica ed Energetica dei Composti di Coordinazione, CNR, Via Jacopo Nardi, 39-50132 Firenze, Italy*

[b] *Dipartimento di Chimica, Università di Siena, Pian dei Mantellini, 44-53100 Siena, Italy*

Monomeric thiolate complexes of formula $[M\{(PPh_2CH_2)_3CMe\}(o\text{-}S_2C_6H_4)][PF_6]_n$ (M = Fe^{II}, Fe^{III}, Co^{II}, Co^{III}, Rh^{II} or Rh^{III}; n = 0 or 1) have been synthesized. The molecular structure of all these compounds has been established by single-crystal X-ray diffraction studies. All the complexes display a square-pyramidal geometry with differing degrees of distortion depending on the oxidation state and electronic configuration of the metal. Electrochemistry served to localize the formal electrode potentials of the different M^{II}–M^{III} couples. In dichloromethane solution, the iron(III) complex (E° = +0.04 V *vs.* saturated calomel electrode) is easier to reduce than the cobalt(III) complex (E° = −0.39 V), which in turn is easier to reduce than the rhodium(III) complex (E° = −0.69 V). In the case of the iron species, the possibility of obtaining the somewhat stable Fe^{I} congener has been realized. The paramagnetic Fe^{I} and Fe^{III}, Co^{II} and Rh^{II} derivatives have been studied by EPR spectroscopy under different experimental conditions, confirming that the unpaired electron is mainly localized on the metal centre. For cobalt and rhodium derivatives EPR results indicate the presence in solution of a chemical equilibrium between two different isomers.

Interest in mono- and poly-nuclear transition-metal thiolates has undergone a remarkable increase in recent years.[1] Metal thiolate complexes are involved in fundamental catalytic (*e.g.* hydrodesulfurization[2]) and biological (*e.g.* iron–sulfur proteins[3]) processes. In particular the study of sulfur–metal centres, associated with several important features such as redox behaviour, unusual geometries, stabilization of uncommon metal oxidation states, electron deficiency or abundance, can contribute to the understanding of structure, bonding and function of biologically important sulfur–metal sites.[3]

We have now synthesized and characterized a series of monomeric thiolate complexes of formula $[M(triphos)(bdt)][PF_6]_n$ [M = Fe, Co or Rh; triphos = 1,1,1-tris(diphenylphosphinomethyl)ethane; bdt = *o*-benzenedithiolate(2−); n = 0 or 1]. In order to detect the structural changes associated with the M^{III}–M^{II} couples, the molecular structures of all these complexes were determined. Since polyphosphine–transition-metal complexes with bis-sulfido coligands usually display good electron-transfer capability,[4–11] we have also examined the electrochemical behaviour of these complexes. In addition all the paramagnetic derivatives have been characterized by EPR spectroscopy.

While this work was in progress the complex $[Co(triphos)(bdt)]^+$, isolated as its tetrafluoroborate salt, was reported.[11] Since the structural parameters of the PF_6 analogue [a = 15.088(7), b = 12.761(7), c = 23.394(7) Å, β = 99.95(5)°, space group $P2_1/c$, Z = 4] match those of the BF_4 complex, we have used the data already published[11] for discussion.

† *Supplementary data available* (No. SUP 57047, 16 pp.): simulations of the EPR spectra. See Instructions for Authors, *J. Chem. Soc., Dalton Trans.*, 1995, Issue 1, pp. xxv–xxx.

Non-SI units employed: G = 10^{-4} T; μ_B = 9.27 × 10^{-24} J T^{-1}.

Experimental

Materials and Methods.—All reactions and manipulations were carried out under a nitrogen atmosphere. Reagent grade chemicals were used in the preparation of the complexes. The $^{31}P\text{-}\{^1H\}$ NMR spectra were recorded on a Bruker AC-200 spectrometer. Peak positions are relative to external phosphoric acid with downfield values reported as positive. Conductivity measurements were carried out with a MTW model LBRIB conductivity bridge. Magnetic susceptibilities of the solid samples were measured on a Faraday balance. Materials and apparatus for the electrochemical and coupled EPR spectroscopic measurements have been described elsewhere.[12,13] Potentials are referred to the saturated calomel electrode (SCE). The diphenylpicrylhydrazyl free radical (dpph) was used as suitable H_0 external magnetic field marker (g_{iso} = 2.0036).

Syntheses.—$[Fe(triphos)(bdt)]\cdot ClCH_2CH_2Cl$ **1**. A solution of $FeCl_2$ (127 mg, 1 mmol) in ethanol (25 cm^3) was added to a solution of triphos (624 mg, 1 mmol) in acetone (20 cm^3), then dropwise addition of a previously prepared solution of $Na_2(bdt)$ (186 mg, 1 mmol) in methanol (15 cm^3) changed the solution from pale green to brown. Sodium chloride was filtered off and the filtrate concentrated under a stream of nitrogen, at room temperature, until gold crystals precipitated. These were collected on a sintered-glass frit, washed with ethanol, then pentane, and dried under a flow of nitrogen. The complex was recrystallized from 1,2-dichloroethane–butanol. Yield 84% (Found: C, 63.85; H, 5.20; Fe, 6.15; S, 6.90. Calc. for $C_{49}H_{47}Cl_2FeP_3S_2$: C, 64.00; H, 5.15; Fe, 6.05; S, 6.95%). $^{31}P\text{-}\{^1H\}$ NMR (CH_2Cl_2, 295 K): δ 55 (s, br).

$[Fe(triphos)(bdt)][PF_6]$ **2**. Addition of solid $[Fe(C_5H_5)_2][PF_6]$ (166 mg, 0.5 mmol) to a brown solution of **1** (413 mg, 0.5 mmol) in CH_2Cl_2 (25 cm^3) gave a deep violet solution. Elution with ethanol (30 cm^3) and solvent evaporation gave

dark violet crystals. The complex was recrystallized from dichloromethane–ethanol. Yield 94% (Found: C, 58.35; H, 4.50; Fe, 5.75; S, 6.50. Calc. for $C_{47}H_{43}F_6FeP_4S_2$: C, 58.45, H, 4.50; Fe, 5.80; S, 6.65%).

[Co(triphos)(bdt)]·CH_2Cl_2 **3**. The complex was prepared by a method analogous to that used for **1**, using $CoCl_2·6H_2O$ as the source of cobalt. The complex was recrystallized from dichloromethane–ethanol to give red-brown crystals. Yield 86% (Found: C, 63.35; H, 5.05; Co, 6.40; S, 7.00. Calc. for $C_{48}H_{45}Cl_2CoP_3S_2$: C, 63.45; H, 5.00; Co, 6.50; S, 7.05%).

[Co(triphos)(bdt)][PF_6] **4**. The complex was prepared by a method analogous to that used for **2** to give dark violet crystals. Yield 95% (Found: C, 58.20; H, 4.55; Co, 6.05; S, 6.50. Calc. for $C_{47}H_{43}CoF_6P_4S_2$: C, 58.25; H, 4.45; Co, 6.10; S, 6.60%). ^{31}P-{^1H} NMR (CH_2Cl_2, 295 K): δ 31.5 (s, br).

[Rh(triphos)(bdt)][PF_6] **5**. A solution of Na_2(bdt) (1.86 mg, 1 mmol) in methanol (15 cm^3) was added, dropwise, at room temperature, to a suspension of [$RhCl_3$(triphos)][14] (833 mg, 1 mmol) in thf (tetrahydrofuran) (20 cm^3) under continuous stirring. The resulting dark violet solution was filtered and [NBu_4][PF_6] (387 mg, 1 mmol), dissolved in ethanol (20 cm^3), was added. Evaporation of the solvent, at room temperature, under a stream of nitrogen, allowed the precipitation of dark violet crystals. These were collected as previously described. The complex was recrystallized from dichloromethane–ethanol. Yield 81% (Found: C, 55.65; H, 4.35; Rh, 10.20; S, 6.25. Calc. for $C_{47}H_{43}F_6P_4RhS_2$: C, 55.75; H, 4.30; Rh, 10.15; S, 6.35%). ^{31}P-{^1H} NMR (CH_2Cl_2, 295 K): δ 31.5 (d, $^1J_{RhP}$ = 100 Hz).

[Rh(triphos)(bdt)]·thf **6**. Addition of an equimolar amount of LiPh (1 mol dm^{-3} thf) or Na($C_{10}H_8$) (1 mol dm^{-3} thf) to a solution of **5** (506 mg, 0.5 mmol) in thf (20 cm^3) changed the dark violet solution to dark green. Elution with butanol (20 cm^3), and evaporation of the solvent gave dark greenish crystals. Yield 92% (Found: C, 65.15; H, 5.55; Rh, 10.85; S, 6.75. Calc. for $C_{51}H_{51}OP_3RhS_2$: C, 65.15; H, 5.45; Rh, 10.95; S, 6.80%).

Complex **6** can be alternatively prepared by the following one-pot reaction. A solution of Na_2(bdt) (1.86 mg, 1 mmol) and NaOMe (540 mg, 10 mmol) in methanol (15 cm^3) was added, dropwise, at room temperature, to a suspension of [$RhCl_3$-(triphos)] (833 mg, 1 mmol) in thf (20 cm^3) under continuous stirring. The resulting solution was filtered and ethanol (20 cm^3) was added. Evaporation of the solvent, at room temperature, under a stream of nitrogen gave dark violet crystals. Yield 89%.

Complex **5** can be obtained by oxidation of **6** with [$Fe(C_5H_5)_2$][PF_6] as described above.

Crystallography.—Diffraction data of all the species **1**–**6** were collected at room temperature; unit-cell parameters were determined from a least-squares refinement of the setting angles of 25 carefully centred reflections. Crystal data and data collection details for the compounds are reported in Table 1. During the data collection the stability of the crystals was checked by periodically measuring three standard reflections: while **2**–**6** did not show any trend, with intensity decay at the end always < 5%, **1** showed a 20% decay. After rescaling and background correction, the intensities were assigned standard deviations σ(I) calculated using a value of 0.03 for the instability factor k.[15] The intensities were corrected for Lorentz-polarization effects and for absorption.[16]

All calculations were carried out on a Hewlett-Packard 486 personal computer using SHELX 76[17] and PLUTO.[18] Atomic scattering factors for non-hydrogen atoms were taken from ref. 19, with those for hydrogen atoms from ref. 20. Both the $\Delta f'$ and $\Delta f''$ components of anomalous dispersion were included for all non-hydrogen atoms.[21]

Since the complexes of both the M^{II} and the M^{III} series are isomorphous only the structure of one complex for each series was solved by the heavy-atom method. Full-matrix least-squares refinements were carried out using anisotropic thermal parameters for the heavier atoms and isotropic for the carbon ones, the function minimized being $\Sigma w(|F_o| - |F_c|)^2$, where w was set equal to $1/\sigma^2(F_o)$. The phenyl rings with the exception of that of bdt were treated as rigid groups of D_{6h} symmetry; the hydrogen atoms were introduced in calculated positions but not refined. Final positional parameters are reported in Tables 2–6.

Additional material available from the Cambridge Crystallographic Data Centre comprises H-atom coordinates, thermal parameters and remaining bond lengths and angles.

Discussion

Complexes **1** and **3** were synthesized by reaction of $FeCl_2$ or $CoCl_2·6H_2O$ with Na_2(bdt), in the presence of equimolar amounts of the ligand triphos. These can be easily oxidized to the species **2** and **4** by reaction with [$Fe(C_5H_5)_2$][PF_6]. The rhodium species **5** is prepared by metathetical reaction of [$RhCl_3$(triphos)] with Na_2(bdt) and [NBu_4][PF_6]. Successive treatment of **5** with a variety of reducing agents such as LiPh or Na($C_{10}H_8$) easily generates the neutral rhodium species **6**. The exposure of solutions of **1** or **6** to air is sufficient to generate **2** or **5**. The reaction of **6** with H^+ (*e.g.* CF_3SO_3H) cleanly generates **5** and H_2. All the complexes are soluble in organic solvents such as dichloromethane, 1,2-dichloroethane, acetone and thf.

The solid compounds **1**, **4** and **5** are diamagnetic, **2**, **3** and **6** are paramagnetic with effective magnetic moments, at room temperature, of 2.00, 1.92 and 2.15 μ_B respectively.

Description of the Structures.—Table 7 reports selected bond distances and angles of all the members of the series. Due to the isomorphism of the M^{III} and M^{II} complexes, the drawings of only two species, [Fe(triphos)(bdt)]$^+$ and [Fe(triphos)(bdt)], are shown in Figs. 1 and 2. In all the complexes the metal is

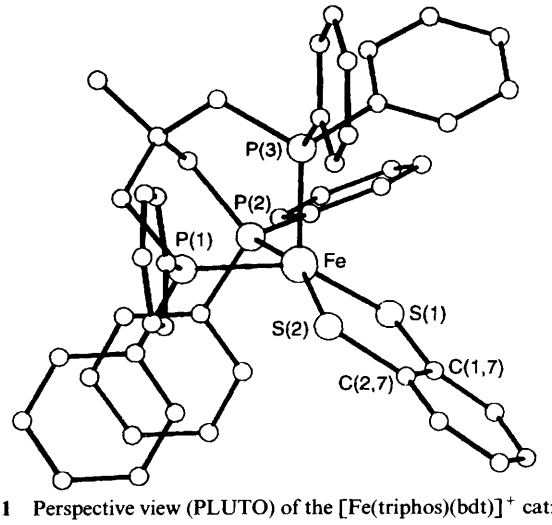

Fig. 1 Perspective view (PLUTO) of the [Fe(triphos)(bdt)]$^+$ cation

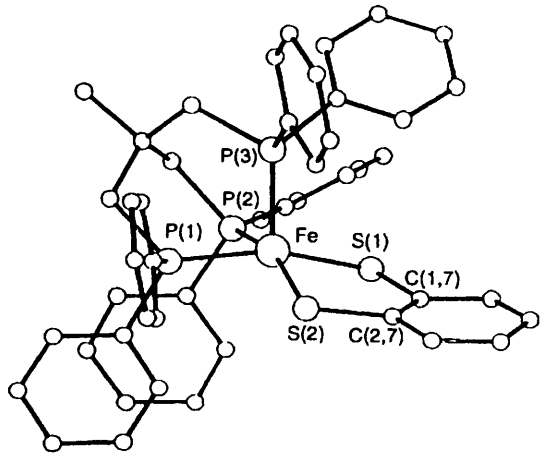

Fig. 2 Perspective view (PLUTO) of the [Fe(triphos)(bdt)] molecule

Table 1 Crystal data and data collection details

	2 d^5	**1** d^6	**3** d^7	**5** d^6	**6** d^7
Formula	$C_{47}H_{43}F_6FeP_4S_2$	$C_{49}H_{47}Cl_2FeP_3S_2$	$C_{48}H_{45}Cl_2CoP_3S_2$	$C_{47}H_{43}F_6P_4RhS_2$	$C_{51}H_{51}OP_3RhS_2$
M	965.73	919.72	908.78	1012.78	939.93
a/Å	15.084(7)	15.282(6)	15.319(6)	15.233(6)	15.615(4)
b/Å	12.842(5)	15.225(5)	15.248(6)	12.721(5)	15.365(4)
c/Å	23.448(9)	18.871(9)	18.877(8)	23.370(9)	18.950(8)
α/°	90	90	90	90	90
β/°	100.04(4)	98.09(5)	96.52(4)	99.88(4)	98.24(4)
γ/°	90	90	90	90	90
U/Å^3	4472.5	4346.9	4380.8	4461.4	4499.6
D_c/g cm^{-3}	1.434	1.405	1.377	1.507	1.387
Colour	Deep violet	Gold	Red-brown	Dark violet	Deep green
Habit	Truncated octahedron	Parallelepiped	Prism	Parallelepiped	Parallelepiped
Crystal dimensions/mm	0.60 × 0.50 × 0.15	0.30 × 0.30 × 0.05	0.30 × 0.20 × 0.025	0.25 × 0.15 × 0.10	0.35 × 0.35 × 0.15
μ/cm^{-1}	6.23	61.65	7.45	6.64	6.03
Absorption correction range (%)	0.94–1.06	0.67–1.26	0.89–1.09	0.91–1.08	0.91–1.21
Diffractometer	Nonius CAD4	Philips PW1100	Nonius CAD4	Nonius CAD4	Nonius CAD4
Radiation (λ/Å)	Mo-Kα (0.7107)	Cu-Kα (1.5418)	Mo-Kα (0.7107)	Mo-Kα (0.7107)	Mo-Kα (0.7107)
Scan speed/° min^{-1}	8.24	4.2–8.4	8.24	8.24	8.24
Scan width/°	0.70 + 0.35 tan θ	1.2 + 0.15 tan θ	0.70 + 0.35 tan θ	0.70 + 0.35 tan θ	0.70 + 0.35 tan θ
2θ range/°	5–45	5–90	5–40	5–45	5–45
Total data	6400	3828	4478	6381	6426
Data used with $I > 3\sigma(I)$	3513	2165	882	2589	3009
Number of variables	242	205	191	242	199
R, R' *	0.052, 0.050	0.082, 0.079	0.056, 0.056	0.041, 0.043	0.047, 0.046

Details in common: space group $P2_1/c$; $Z = 4$; graphite-monochromated radiation; scan mode ω–2θ. * $R = \Sigma||F_o| - |F_c||/|F_o|$, $R' = [\Sigma w(|F_o| - |F_c|)^2/\Sigma w|F_o|^2]^{\frac{1}{2}}$.

Table 2 Atomic coordinates (× 10^4) for [Fe(triphos)(bdt)][PF_6]

Atom	*x*	*y*	*z*
Fe	3232(1)	2241(1)	1041(1)
P(1)	1883(1)	2957(1)	653(1)
P(2)	2739(1)	2239(1)	1919(1)
P(3)	2622(1)	659(1)	816(1)
P(4)	8963(2)	3627(2)	2238(1)
S(1)	4577(1)	2423(2)	1532(1)
S(2)	3711(1)	2830(2)	293(1)
F(1)	8908(4)	3674(5)	2895(2)
F(2)	9032(5)	3615(6)	1576(3)
F(3)	8328(6)	2740(6)	2123(4)
F(4)	9797(5)	2933(8)	2356(3)
F(5)	8152(5)	4406(6)	2110(3)
F(6)	9544(6)	4638(7)	2297(4)
C(1)	150(5)	997(6)	1395(3)
C(2)	1074(4)	1387(5)	1296(3)
C(3)	922(4)	2398(5)	940(3)
C(4)	1653(4)	1585(5)	1892(3)
C(5)	1474(4)	514(5)	972(3)
C(1,1)	1817(3)	4358(4)	775(2)
C(2,1)	978(3)	4846(4)	680(2)
C(3,1)	917(3)	5916(4)	769(2)
C(4,1)	1695(3)	6498(4)	953(2)
C(5,1)	2534(3)	6010(4)	1048(2)
C(6,1)	2595(3)	4940(4)	959(2)
C(1,2)	1516(3)	2893(3)	−135(2)
C(2,2)	1739(3)	3719(3)	−473(2)
C(3,2)	1468(3)	3696(3)	−1073(2)
C(4,2)	973(3)	2853(3)	−1335(2)
C(5,2)	750(3)	2032(3)	−996(2)
C(6,2)	1021(3)	2055(3)	−396(2)
C(1,3)	3410(3)	1642(3)	2563(2)
C(2,3)	3212(3)	1927(3)	3101(2)
C(3,3)	3650(3)	1437(3)	3603(2)
C(4,3)	4286(3)	663(3)	3567(2)
C(5,3)	4484(3)	378(3)	3029(2)
C(6,3)	4046(3)	868(3)	2527(2)
C(1,4)	2623(2)	3575(3)	2177(2)
C(2,4)	1796(2)	4058(3)	2181(2)
C(3,4)	1767(2)	5087(3)	2368(2)
C(4,4)	2565(2)	5632(3)	2551(2)
C(5,4)	3392(2)	5149(3)	2548(2)
C(6,4)	3422(2)	4120(3)	2361(2)
C(1,5)	3311(3)	−342(4)	1231(2)
C(2,5)	3031(3)	−955(4)	1658(2)
C(3,5)	3597(3)	−1726(4)	1938(2)
C(4,5)	4444(3)	−1885(4)	1791(2)
C(5,5)	4725(3)	−1273(4)	1364(2)
C(6,5)	4158(3)	−501(4)	1085(2)
C(1,6)	2524(3)	80(3)	98(2)
C(2,6)	2816(3)	561(3)	−370(2)
C(3,6)	2710(3)	59(3)	−905(2)
C(4,6)	2313(3)	−925(3)	−972(2)
C(5,6)	2021(3)	−1406(3)	−505(2)
C(6,6)	2127(3)	−903(3)	30(2)
C(1,7)	5256(4)	2879(5)	1060(3)
C(2,7)	4858(4)	3069(5)	495(3)
C(3,7)	5366(6)	3444(7)	96(4)
C(4,7)	6287(6)	3661(7)	291(4)
C(5,7)	6673(6)	3492(6)	855(3)
C(6,7)	6173(5)	3101(6)	1245(3)

Table 3 Atomic coordinates (× 10^4) for [Fe(triphos)(bdt)]·ClC_2H_4Cl

Atom	*x*	*y*	*z*
Fe	3171(2)	523(1)	1474(1)
P(1)	3098(3)	1731(3)	830(2)
P(2)	4270(3)	1106(3)	2187(2)
P(3)	2217(3)	1030(3)	2099(2)
S(1)	3545(3)	−763(2)	1923(2)
S(2)	2475(3)	−164(3)	538(2)
C(1)	3216(11)	3579(10)	2491(9)
C(2)	3195(10)	2637(9)	2173(8)
C(3)	3243(10)	2740(9)	1375(8)
C(4)	4022(10)	2175(9)	2559(8)
C(5)	2332(10)	2222(9)	2308(8)
C(1,1)	2112(6)	1928(6)	190(5)
C(2,1)	2060(6)	1603(6)	−506(5)
C(3,1)	1291(6)	1724(6)	−989(5)
C(4,1)	574(6)	2170(6)	−777(5)
C(5,1)	626(6)	2495(6)	−81(5)
C(6,1)	1395(6)	2374(6)	403(5)
C(1,2)	3891(6)	1889(5)	213(5)
C(2,2)	4013(6)	2728(5)	−53(5)
C(3,2)	4650(6)	2869(5)	−502(5)
C(4,2)	5166(6)	2172(5)	−685(5)
C(5,2)	5044(6)	1332(5)	−419(5)
C(6,2)	4407(6)	1191(5)	30(5)
C(1,3)	5224(7)	1313(5)	1743(5)
C(2,3)	5537(7)	2147(5)	1603(5)
C(3,3)	6273(7)	2235(5)	1247(5)
C(4,3)	6696(7)	1489(5)	1031(5)
C(5,3)	6382(7)	655(5)	1172(5)
C(6,3)	5647(7)	567(5)	1528(5)
C(1,4)	4830(6)	565(5)	3006(5)
C(2,4)	5706(6)	789(5)	3252(5)
C(3,4)	6129(6)	435(5)	3891(5)
C(4,4)	5678(6)	−143(5)	4284(5)
C(5,4)	4803(6)	−367(5)	4038(5)
C(6,4)	4379(6)	−13(5)	3399(5)
C(1,5)	1045(7)	982(7)	1807(6)
C(2,5)	684(7)	449(7)	1239(6)
C(3,5)	−231(7)	406(7)	1047(6)
C(4,5)	−784(7)	897(7)	1424(6)
C(5,5)	−422(7)	1430(7)	1991(6)
C(6,5)	492(7)	1473(7)	2183(6)
C(1,6)	2192(7)	498(5)	2966(6)
C(2,6)	2365(7)	911(5)	3631(6)
C(3,6)	2372(7)	423(5)	4258(6)
C(4,6)	2206(7)	−478(5)	4219(6)
C(5,6)	2033(7)	−891(5)	3554(6)
C(6,6)	2026(7)	−403(5)	2928(6)
C(1,7)	2881(9)	−1502(9)	1407(8)
C(2,7)	2377(10)	−1250(10)	783(8)
C(3,7)	1843(10)	−1841(10)	365(9)
C(4,7)	1792(11)	−2685(11)	631(9)
C(5,7)	2228(10)	−2934(11)	1284(9)
C(6,7)	2790(11)	−2369(10)	1681(9)
Cl(1)*	8818(7)	−147(5)	4232(5)
Cl(2)*	9743(5)	−1393(5)	3133(5)
C(6)*	9741(18)	159(18)	3783(16)
C(7)*	9647(18)	−255(19)	3133(16)

* 1,2-Dichloroethane solvent.

surrounded by the phosphorus atoms of the triphos ligand and by the sulfur atoms of the thiolate in a distorted square-pyramidal environment, with one phosphorus, P(3) in the apical position. The distortion of the square pyramid, which is well evidenced by the values of the basal angles [149.3(1)–165.6(1)°], varies to a certain extent going from one species to another. Taking into account that the geometry of the P_3M fragment is essentially fixed by the steric demands of the tripod ligand to a hemioctahedron with all the P–M–P angles very close to 90°, the different degree of distortion reflects essentially on the bond angles involving the thiolate ligand. Indeed none of the sulfur atoms of the bdt ligand lies on the MP(1)P(2) planes as evidenced by the deviations of the sulfur atoms from the latter planes which range from 0.58 to 1.08 Å. It follows that the MP(1)P(2) planes make angles with the MS(1)S(2) ones which average 34.3 and 25.1° in the M^{III} and M^{II} complexes respectively. These values together with those of the *trans* basal angles indicate that all the M^{III} complexes deviate from square-pyramidal geometry more than the M^{II} ones. An even larger difference between the oxidized and reduced forms can be noted in the steric arrangement of the phenyl group of the thiolate. In the oxidized species this group is disposed essentially planar

Table 4 Atomic coordinates (× 10^4) for [Co(triphos)(bdt)]·CH_2Cl_2

Atom	x	y	z
Co	3183(3)	503(3)	1504(2)
P(1)	3096(5)	1716(5)	863(4)
P(2)	4284(5)	1107(5)	2203(4)
P(3)	2143(5)	1036(5)	2186(4)
S(1)	3554(5)	−800(5)	1964(4)
S(2)	2489(5)	−194(5)	569(4)
C(1)	3252(19)	3560(19)	2524(16)
C(2)	3202(17)	2629(17)	2214(13)
C(3)	3232(17)	2729(17)	1418(13)
C(4)	3985(17)	2134(16)	2603(14)
C(5)	2327(18)	2236(18)	2396(14)
C(1,1)	2102(10)	1903(11)	248(10)
C(2,1)	2082(10)	1562(11)	−440(10)
C(3,1)	1327(10)	1652(11)	−922(10)
C(4,1)	593(10)	2083(11)	−718(10)
C(5,1)	612(10)	2423(11)	−30(10)
C(6,1)	1367(10)	2333(11)	453(10)
C(1,2)	3924(10)	1885(10)	232(9)
C(2,2)	4022(10)	2724(10)	−44(9)
C(3,2)	4642(10)	2874(10)	−517(9)
C(4,2)	5164(10)	2186(10)	−715(9)
C(5,2)	5066(10)	1348(10)	−438(9)
C(6.2)	4446(10)	1197(10)	35(9)
C(1,3)	5239(11)	1349(10)	1731(9)
C(2,3)	5530(11)	2197(10)	1608(9)
C(3,3)	6259(11)	2323(10)	1240(9)
C(4,3)	6698(11)	1602(10)	994(9)
C(5,3)	6407(11)	755(10)	1117(9)
C(6,3)	5677(11)	628(10)	1485(9)
C(1,4)	4839(11)	558(10)	2991(9)
C(2,4)	5714(11)	765(10)	3215(9)
C(3,4)	6126(11)	417(10)	3850(9)
C(4,4)	5663(11)	−138(10)	4261(9)
C(5,4)	4788(11)	−345(10)	4037(9)
C(6,4)	4376(11)	3(10)	3401(9)
C(1,5)	962(13)	1001(12)	1910(10)
C(2,5)	606(13)	504(12)	1327(10)
C(3,5)	−300(13)	501(12)	1131(10)
C(4,5)	−850(13)	994(12)	1518(10)
C(5,5)	−493(13)	1491(12)	2101(10)
C(6,5)	413(13)	1494(12)	2297(10)
C(1,6)	2133(11)	520(10)	3060(11)
C(2,6)	2280(11)	945(10)	3717(11)
C(3,6)	2275(11)	468(10)	4347(11)
C(4,6)	2124(11)	−435(10)	4320(11)
C(5,6)	1978(11)	−860(10)	3663(11)
C(6,6)	1982(11)	−382(10)	3033(11)
C(1,7)	2852(18)	−1532(20)	1487(16)
C(2,7)	2370(17)	−1270(18)	852(13)
C(3,7)	1804(19)	−1824(21)	466(16)
C(4,7)	1748(20)	−2661(24)	707(16)
C(5,7)	2162(19)	−2963(23)	1375(16)
C(6,7)	2749(18)	−2381(20)	1776(15)
C(6)*	211(32)	4924(33)	1551(25)
Cl(1)*	330(12)	3813(12)	1959(9)
Cl(2)*	953(13)	4834(14)	926(11)

* Methylene chloride solvent.

Table 5 Atomic coordinates (× 10^4) for [Rh(triphos)(bdt)][PF_6]

Atom	x	y	z
Rh	3202(1)	2276(1)	1055(1)
P(1)	1841(2)	2967(2)	651(1)
P(2)	2732(2)	2223(2)	1944(1)
P(3)	2640(2)	665(2)	845(1)
P(4)	8979(2)	3607(3)	2227(2)
S(1)	4641(2)	2324(3)	1538(1)
S(2)	3737(2)	2980(3)	283(1)
F(1)	8903(5)	3637(7)	2884(3)
F(2)	9065(7)	3596(7)	1568(3)
F(3)	8363(8)	2708(9)	2103(5)
F(4)	9810(6)	2936(10)	2353(4)
F(5)	8188(7)	4386(8)	2094(4)
F(6)	9556(9)	4619(10)	2307(5)
C(1)	179(6)	962(8)	1407(4)
C(2)	1091(6)	1376(8)	1314(4)
C(3)	910(6)	2379(8)	954(4)
C(4)	1651(6)	1579(8)	1917(4)
C(5)	1500(6)	511(8)	989(4)
C(1,1)	1768(4)	4367(5)	776(3)
C(2,1)	928(4)	4836(5)	689(3)
C(3,1)	849(4)	5914(5)	777(3)
C(4,1)	1610(4)	6523(5)	951(3)
C(5,1)	2450(4)	6054(5)	1037(3)
C(6,1)	2529(4)	4976(5)	950(3)
C(1,2)	1493(4)	2881(5)	−133(3)
C(2,2)	1735(4)	3698(5)	−472(3)
C(3,2)	1479(4)	3670(5)	−1075(3)
C(4,2)	982(4)	2826(5)	−1338(3)
C(5,2)	739(4)	2009(5)	−998(3)
C(6,2)	995(4)	2036(5)	−396(3)
C(1,3)	3403(4)	1612(4)	2580(3)
C(2,3)	3213(4)	1885(4)	3124(3)
C(3,3)	3652(4)	1379(4)	3622(3)
C(4,3)	4281(4)	600(4)	3575(3)
C(5,3)	4470(4)	327(4)	3031(3)
C(6,3)	4031(4)	832(4)	2534(3)
C(1,4)	2633(3)	3562(5)	2197(3)
C(2,4)	1819(3)	4060(5)	2204(3)
C(3,4)	1801(3)	5105(5)	2382(3)
C(4,4)	2596(3)	5652(5)	2553(3)
C(5,4)	3410(3)	5154(5)	2546(3)
C(6,4)	3429(3)	4109(5)	2368(3)
C(1,5)	3321(4)	−364(5)	1239(3)
C(2,5)	4146(4)	−547(5)	1073(3)
C(3,5)	4703(4)	−1335(5)	1346(3)
C(4,5)	4437(4)	−1940(5)	1784(3)
C(5,5)	3612(4)	−1757(5)	1949(3)
C(6,5)	3055(4)	−969(5)	1676(3)
C(1,6)	2539(5)	146(5)	114(3)
C(2,6)	2840(5)	655(5)	−344(3)
C(3,6)	2724(5)	186(5)	−892(3)
C(4,6)	2308(5)	−792(5)	−980(3)
C(5,6)	2007(5)	−1300(5)	−522(3)
C(6,6)	2122(5)	−831(5)	26(3)
C(1,7)	5281(6)	2833(8)	1051(4)
C(2,7)	4875(6)	3075(8)	491(4)
C(3,7)	5406(8)	3503(10)	109(5)
C(4,7)	6305(8)	3656(10)	295(5)
C(5,7)	6704(8)	3399(9)	845(5)
C(6,7)	6198(7)	2967(8)	1228(4)

with the MS(1)S(2) plane [dihedral angles MS(1)S(2)/S(1)S(2)Ph always < 1°], whilst in the reduced forms there is a strong folding of the ring along the S(1)S(2) vector toward the apical ligand, with dihedral angles MS(1)S(2)/S(1)S(2)Ph in the range 17.5–19.4°. Previously the folding of the chelate ring, which shows a large variation of distortion in the numerous bdt complexes reported, has been often ascribed to packing effects as well as to π-bonding interactions.[22,23] In the present series the electronic factor seems important as we can correlate the folding of the chelate ring with the electronic density at the metal centre. It is possible that a conjugative system, which becomes important in stabilizing the oxidized form, is removed when more electron density is available at the metal centre.

Concerning the bond distances within the co-ordination polyhedra the following features are noted: (*i*) In the d^6–d^7 redox couples, namely Co and Rh, on going from d^6 to d^7 there is a lengthening of the apical M–P bond distance and, if the different covalent radii of the metals are taken into account, this lengthening occurs to the same extent, being *ca.* 0.12 Å in both cases. In a molecular orbital picture the lengthening of the $M–P_{apical}$ bond in a d^7 species with square-pyramidal geometry

Table 6 Atomic coordinates ($\times 10^4$) for [Rh(triphos)(bdt)]·C_4H_8O

Atom	*x*	*y*	*z*
Rh	3231(1)	472(1)	1461(1)
P(1)	3154(2)	1723(2)	807(1)
P(2)	4359(2)	1093(2)	2191(1)
P(3)	2215(2)	1041(2)	2148(1)
S(1)	3566(2)	−901(2)	1944(1)
S(2)	2457(2)	−262(2)	492(1)
C(1)	3300(7)	3540(7)	2485(6)
C(2)	3254(6)	2613(6)	2177(5)
C(3)	3280(6)	2716(6)	1366(5)
C(4)	4038(6)	2129(6)	2563(5)
C(5)	2409(6)	2213(6)	2332(5)
C(1,1)	2169(4)	1889(4)	171(4)
C(2,1)	2133(4)	1562(4)	−519(4)
C(3,1)	1372(4)	1635(4)	−1000(4)
C(4,1)	647(4)	2035(4)	−791(4)
C(5,1)	683(4)	2361(4)	−100(4)
C(6,1)	1444(4)	2289(4)	381(4)
C(1,2)	3951(3)	1894(3)	206(3)
C(2,2)	4068(3)	2728(3)	−56(3)
C(3,2)	4690(3)	2872(3)	−504(3)
C(4,2)	5194(3)	2182(3)	−689(3)
C(5,2)	5077(3)	1349(3)	−427(3)
C(6,2)	4456(3)	1205(3)	21(3)
C(1,3)	5299(4)	1334(3)	1748(3)
C(2,3)	5588(4)	2171(3)	1623(3)
C(3,3)	6301(4)	2286(3)	1265(3)
C(4,3)	6723(4)	1564(3)	1032(3)
C(5,3)	6434(4)	727(3)	1157(3)
C(6,3)	5722(4)	612(3)	1515(3)
C(1,4)	4893(3)	558(4)	3002(3)
C(2,4)	5751(3)	764(4)	3263(3)
C(3,4)	6144(3)	409(4)	3906(3)
C(4,4)	5679(3)	−152(4)	4289(3)
C(5,4)	4822(3)	−358(4)	4029(3)
C(6,4)	4429(3)	−3(4)	3386(3)
C(1,5)	1044(5)	1034(5)	1852(4)
C(2,5)	701(5)	483(5)	1298(4)
C(3,5)	−191(5)	457(5)	1079(4)
C(4,5)	−739(5)	983(5)	1415(4)
C(5,5)	−396(5)	1534(5)	1969(4)
C(6,5)	496(5)	1560(5)	2188(4)
C(1,6)	2215(4)	517(3)	3018(4)
C(2,6)	2367(4)	938(3)	3676(4)
C(3,6)	2368(4)	465(3)	4304(4)
C(4,5)	2217(4)	−430(3)	4275(4)
C(5,6)	2065(4)	−852(3)	3617(4)
C(6,6)	2064(4)	−378(3)	2988(4)
C(1,7)	2832(6)	−1588(6)	1445(5)
C(2,7)	2361(6)	−1330(6)	804(5)
C(3,7)	1779(7)	−1910(7)	400(6)
C(4,7)	1683(7)	−2758(7)	656(6)
C(5,7)	2148(7)	−3020(8)	1300(6)
C(6,7)	2721(7)	−2438(7)	1722(6)
C(6)*	1010(22)	3898(21)	1646(17)
C(7)*	1466(21)	4522(24)	1424(18)
C(8)*	859(21)	4715(21)	817(17)
C(9)*	197(19)	5099(21)	1277(17)
C(10)*	346(21)	4327(23)	1866(17)

* Tetrahydrofuran solvent.

is not surprizing and fits well with the partial occupation of a molecular orbital (metal z^2), which is antibonding in character with respect to M–P(3). (*ii*) In both species of the Fe d^5–d^6 redox couple the apical bonds are shorter than the basal ones, following the general prediction for d^n metal complexes in square-pyramidal geometry (*i.e.* stronger axial than equatorial linkage for $n \leqslant 6$ and the reverse for $n > 6$).[24] The addition of one electron to the d^5 species causes a significant shortening (*ca.* 0.1 Å) of all the Fe–P distances. In particular, for the apical bond in the d^6 case, the possibility of a better interaction between the π accepting orbitals of the apical phosphine and the filled metal d orbitals has to be considered. Indeed the highest occupied molecular orbital in the P_3M fragment is reminiscent of one octahedral t_{2g} lone pair and may backdonate electron density into a proper phosphine orbital.[24] The related Fe^{II} square-pyramidal complex [$Fe(PMe_3)_3$(bdt)], where three monodentate phosphines replace the tripod ligand, shows structural parameters fully comparable with those of [Fe(triphos)(bdt)], with axial and basal Fe–P bond lengths of 2.145(3) and 2.228(5) Å respectively.[25] (*iii*) In all of the couples, on going from the oxidized to the reduced forms, there is a strengthening of the M–P basal bonds with a weakening of the M–S ones. The lengthening of the M–S bonds, which is probably attributable to a varied (increased) π* interaction between the metal d and sulfur p orbitals,[26] is also in agreement with the idea of an interruption of the conjugative system, as appears from the bending of the five-membered ring MS(1)S(2)C(1,7)C(2,7) in the reduced forms. (*iv*) The values of the S–C bond distances, which may be useful in assessing the relative importance of the reduced and oxidized forms of the bdt ligand, do not give any indication of trend in the series of the complexes studied. The lengths of the S–C bonds, 1.722(7)–1.759(9) Å, somewhat shorter than expected for a single bond (1.78 Å), do not differ significantly through the series and fall within the extremes reported in literature for S–C bonds in bdt *i.e.* 1.648 Å in $S_2C_6H_4$ and 1.763 Å in $S_2C_6H_4^{2-}$.[27]

Electrochemistry of the Iron Complexes.—Fig. 3 shows the cyclic voltammetric profiles exhibited by the Fe^{III} complex **2** in dichloromethane solution. Two consecutive redox steps are displayed, possessing features of chemical reversibility. A quite similar voltammetric pattern is exhibited by the Fe^{II} complex **1** (the most anodic step now appears as an oxidation process), thus indicating that the first redox change belongs to the Fe^{III}–Fe^{II} couple. Controlled-potential coulometric tests ($E_{working}$ = −0.5 V) confirm the chemical reversibility of this one-electron step on the macroelectrolysis time-scale too. Analysis[28] of the relevant cyclic voltammograms at different scan rates shows that: (*i*) the $i_{p(backward)}:i_{p(forward)}$ ratio is constantly equal to 1; (*ii*) the peak-to-peak separation increases progressively from 66 mV at 0.02 V s^{-1} to 118 mV at 1.00 V s^{-1}; (*iii*) the current function $i_{p(forward)}v^{-\frac{1}{2}}$ remains substantially constant. Under the same experimental conditions, the one-electron oxidation of ferrocene (E° = +0.45 V) displays quite similar diagnostic parameters, thus suggesting that the **2**–**1** redox change is chemically as well as electrochemically reversible. This suggests that in solution only minor structural reorganization occurs upon one-electron removal/addition processes, as happens in the solid state.

More unexpected is the most cathodic step, which, based on its peak-height, also involves the addition of one electron per molecule. The relevant cyclovoltammetric analysis shows that the $i_{pa}:i_{pc}$ ratio, which is equal to 0.6 at 0.02 V s^{-1}, reaches 0.9 at 5.12 V s^{-1}, thus indicating that the primarily electrogenerated species [Fe(triphos)(bdt)]$^-$ is only transient ($t_{\frac{1}{2}}$ 10 s at 293 K). Based either on EPR measurements (see below) or on the consideration that the 'non-innocent' *o*-benzenedithiolate ligand can be only oxidized stepwise to *o*-dithiobenzoquinone, the [Fe(triphos)(bdt)]$^-$ anion was assigned an Fe^I nature. Although the ability of tripodal polyphosphines to stabilize iron(I) complexes is not new,[29] it must be recognized that they are still rare products.[29,30]

The formal electrode potentials for the Fe^{III}–Fe^{II}–Fe^I sequence are compiled in Table 8.

Electrochemistry of the Cobalt Complexes.—The cyclic voltammetric response exhibited by the Co^{III} complex **4** in dichloromethane solution consists of a chemically and electrochemically reversible Co^{III}–Co^{II} redox change, Table 8. Also in this case the Co^{II} complex **3** gives a fully complementary response. This result is in good agreement with the

Table 7 Selected bond distances (Å) and angles (°) for complexes **1–6**

	2 d^5	**1** d^6	**4*** d^6	**3** d^7	**5** d^6	**6** d^7
M–P(1)	2.273(2)	2.198(4)	2.219(2)	2.205(9)	2.300(3)	2.280(3)
M–P(2)	2.309(2)	2.188(4)	2.245(2)	2.219(8)	2.312(3)	2.286(2)
M–P(3)	2.254(2)	2.145(5)	2.183(2)	2.307(9)	2.244(3)	2.361(3)
M–S(1)	2.164(2)	2.177(4)	2.164(2)	2.216(9)	2.287(2)	2.330(3)
M–S(2)	2.146(2)	2.193(4)	2.174(2)	2.225(8)	2.285(2)	2.339(3)
P(1)–M–P(2)	87.2(1)	88.6(2)	90.0(1)	88.5(3)	89.0(1)	87.3(1)
P(1)–M–P(3)	88.3(1)	91.0(2)	90.4(1)	90.5(3)	88.6(1)	90.0(1)
P(1)–M–S(1)	149.3(1)	163.2(2)	151.4(1)	164.4(4)	155.8(1)	165.6(1)
P(1)–M–S(2)	86.4(1)	88.5(1)	85.5(1)	88.4(3)	86.9(1)	90.0(1)
P(2)–M–P(3)	91.5(1)	92.2(2)	92.9(1)	92.8(3)	90.2(1)	91.8(1)
P(2)–M–S(1)	86.7(1)	89.3(2)	85.4(2)	89.7(3)	88.6(1)	91.7(1)
P(2)–M–S(2)	159.3(1)	158.8(2)	158.8(2)	158.8(4)	158.2(1)	160.6(1)
P(3)–M–S(1)	121.9(1)	105.7(2)	118.0(2)	105.0(3)	115.5(1)	104.4(1)
P(3)–M–S(2)	108.0(1)	108.9(2)	107.8(2)	108.2(3)	111.1(1)	107.4(1)
S(1)–M–S(2)	88.8(1)	87.5(2)	88.7(1)	87.7(3)	86.4(9)	86.2(1)
MP(1)P(2)–MS(1)S(2)	36.7	26.7	34.1	26.0	32.1	23.6
MS(1)S(2)–S(1)S(2)Ph	0.9	17.5	0.8	19.4	0.8	17.6

* The structural parameters of the Co^{III} species are those reported in literature [11] for [Co(triphos)(bdt)][BF_4].

Table 8 Electrochemical characteristics of the redox changes exhibited by $[M(triphos)(bdt)]^{n+}$ (n = 1 or 0), in dichloromethane solution

M	$E°_{+/0}$/V *vs.* SCE	$\Delta E_p{}^a$/mV	$E°_{0/-}$/V *vs.* SCE	$\Delta E_p{}^a$/mV
Fe	+0.04	78	−1.70[b]	78
Co	−0.39	70	—	
	−0.37[c]	112	—	
Rh	−0.69	70	−1.53[a,d]	—

[a] Measured at 0.2 V s^{-1}. [b] Complicated by subsequent chemical reactions; measured at 5.12 V s^{-1}. [c] From ref. 11. [d] Peak-potential value for irreversible processes.

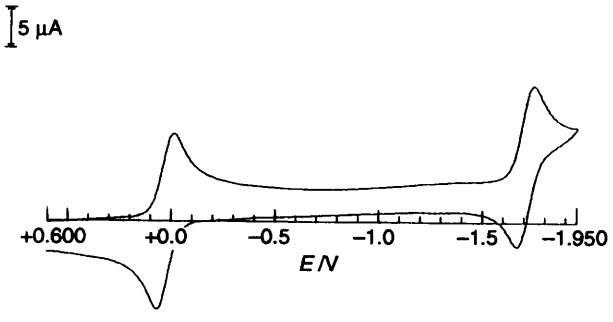

Fig. 3 Cyclic voltammogram recorded at a platinum electrode in CH_2Cl_2 solution containing **2** (8.3 × 10^{-4} mol dm^{-3}) and [NBu_4][ClO_4] (0.2 mol dm^{-3}); scan rate 0.2 V s^{-1}

findings of Huttner and co-workers [11] for [Co(triphos)(bdt)][BF_4].

Electrochemistry of the Rhodium Complexes.—Fig. 4 illustrates the cyclic voltammetric responses exhibited by **5** in dichloromethane solution. Like its Co^{III} analogue, the Rh^{III} complex exhibits a chemically and electrochemically reversible reduction to the corresponding Rh^{II} species. At variance with the Co^{III} species the Rh^{I} oxidation state is also accessible, but unlike the Fe^{I} species it is quite unstable, in that even at 10.24 V s^{-1} no directly associated reoxidation process could be detected in the reverse scan, other than the very far oxidation peak at E_p −0.4 V. As in the preceding cases, the reduced complex **6** gives rise to a cyclic voltammetric profile quite complementary to that shown in Fig. 4. The relevant redox potentials are summarized in Table 8.

Electron Paramagnetic Resonance of the Iron Complexes.—Fig. 5(*a*) shows the X-band EPR glassy spectrum of **2** in dichloromethane solution. The spectrum displays a metal-in-character rhombic lineshape, with g_{aniso} values ($g_l \gg g_m > g_h \neq g_e$; l = low, m = medium, h = high) which are indicative of orbital contribution. The partially resolved superhyperfine structure is consistent with two, partially overlapped 1:3:3:1 pseudo-quadruplets arising from the interaction of the $S = \frac{1}{2}$ electron with the P nuclei of the triphos moiety. The lack of resolution in the g_l region as well as the concomitant poor resolution of the high-field signals indicates the non-complete equivalence of the phosphorus atoms, in agreement with solid-state findings.

Raising the temperature to the glassy-fluid transition induces line broadening and concomitant loss of intensity, likely as a consequence of temperature-dependent dynamics of the co-ordination polyhedron. This spectral behaviour is temperature reversible. The powder spectrum of **2** is similar to the corresponding one of the frozen solution, with a narrow and partially structured rhombic lineshape. This indicates the same co-ordination geometry both in the solid state and in solution. The computer simulated [31] parameters are collected in Table 9.

Fig. 5(*b*) shows the glassy spectrum of the monoanion $[Fe^{I}(triphos)(bdt)]^-$ obtained by electrochemical reduction of **1** at 253 K. The lineshape, typical of a $S = \frac{1}{2}$ metal-centred system with a narrow and unresolved axial structure ($g_{\parallel} > g_{\perp} \approx g_e$) displays a minor orbital contribution in comparison with that of complex **2**.[32] Raising the temperature to the glassy-fluid transition rapidly decreases the intensity of the signal and the fluid solution is EPR silent in the overall range 178–300 K. Refreezing induces only partial recovery of the glassy signals. The remarkable changes in the g_i and a_i anisotropic parameters (Table 9) on passing from the d^5 to the d^7 low-spin iron species suggest that significant deformation of the co-ordination polyhedron occurs, in spite of the electrochemical indication that the Fe^{I} derivative basically maintains the original square-pyramidal geometry.

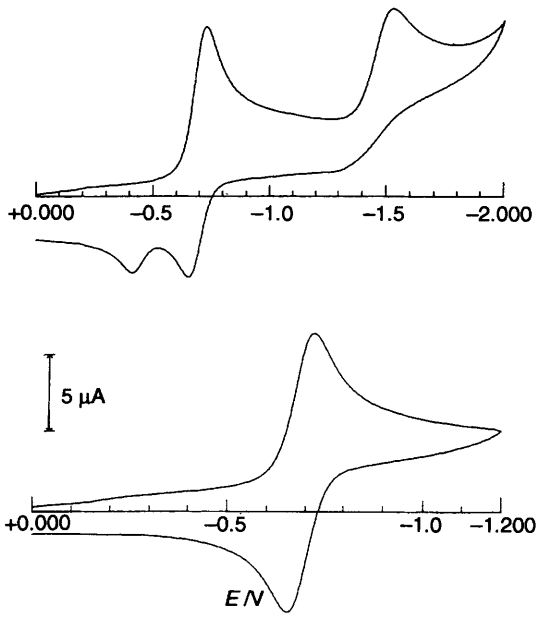

Fig. 4 Cyclic voltammograms recorded at a platinum electrode in CH_2Cl_2 solution containing **5** (7.9×10^{-4} mol dm^{-3}) and $[NBu_4][ClO_4]$ (0.2 mol dm^{-3}); scan rate 0.2 V s^{-1}

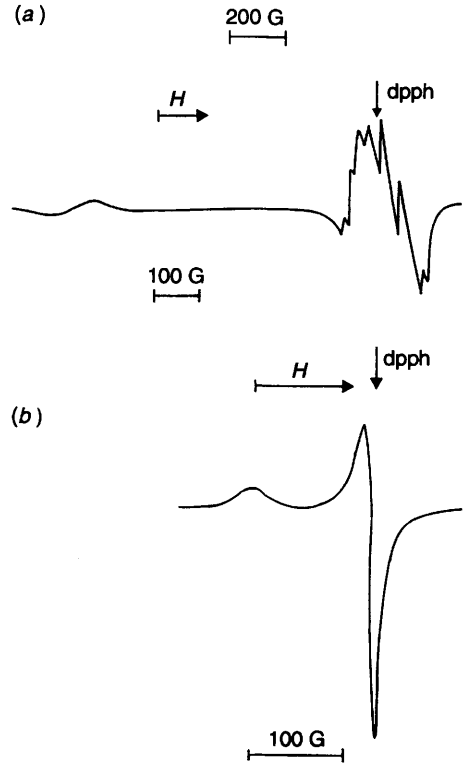

Fig. 5 X-Band EPR spectra of **2** (*a*) second derivative and $[Fe(triphos)(bdt)]^-$ (*b*) in CH_2Cl_2 solution at $T = 100$ K

Electron Paramagnetic Resonance of the Cobalt(II) *Complex*.—Fig. 6 shows the X-band EPR spectra of **3** in dichloromethane solution. The lineshape analysis of the frozen solution, Fig. 6(*a*), is characteristic of a $S = \frac{1}{2}$ spin Hamiltonian with the unpaired electron strongly coupled to the cobalt nucleus (Co, $I = \frac{7}{2}$) in a complex rhombic structure. The overall lineshape exhibits noticeable dependence on the anisotropic m_I(Co) values.[33] The three g_{aniso} regions exhibit different overlapped broad Co hyperfine splittings, with significant orbital contribution. The

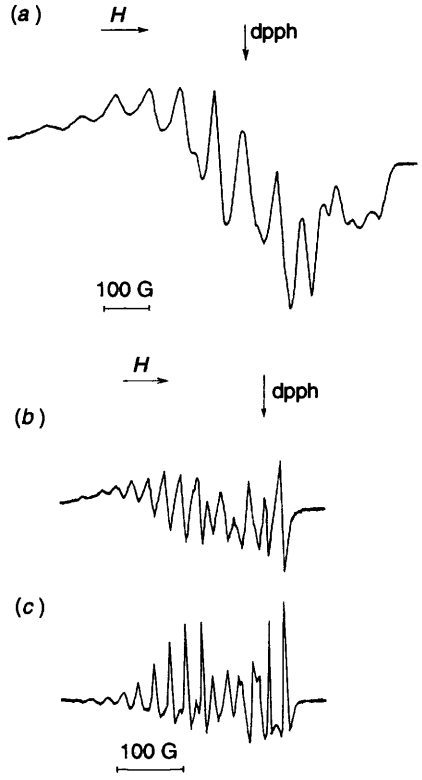

Fig. 6 X-Band EPR spectra of **3** in CH_2Cl_2 solution at $T = 100$ (*a*) and 270 (*b*), (*c*); (*c*) second derivative

intensity of the signal is markedly temperature dependent and for $T > 155$ K the sample becomes EPR silent. Above the glassy-fluid transition the signal is again recovered exhibiting the best resolution at $T = 270$ K, Fig. 6(*b*) and 6(*c*). The metal-centred lineshape is however constituted by two major, partially overlapping ($g_{iso} > g_e$) sets of broad Co^{II} hyperfine signals, likely attributable to two isomeric complexes present in almost equimolar amounts (A and B).[34,35] The lack of any phosphorus superhyperfine splitting in the two multiplets seems to indicate that structural reorganization takes place in solution. An alternative interpretation of the fluid solution spectrum, which assumes a very large superhyperfine coupling with one phosphorus nucleus ($a_{iso} = 150$ G), appears less reliable on the basis of the ratio of the heights of the narrower signals ($m_I = \frac{7}{2}$). Table 9 summarizes the most important EPR features.

Electron Paramagnetic Resonance of the Rhodium(II) *Complex*.—Fig. 7 shows the X-band EPR spectra of **6** in CH_2Cl_2 solution. The glassy lineshape, Fig. 7(*a*), displays three groups of anisotropic signals. The two more intense high-field absorptions can be attributed to one $S = \frac{1}{2}$ metal-centred species (A) in a poorly resolved rhombic structure ($g_l > g_m > g_h$) with some orbital contribution. The minor low-field signal indicates the presence of a second species (B) in lower concentration, with the high-field component probably overlapping the species A. The second derivative of the (A) anisotropic absorptions displays poorly resolved and partially overlapped 1:1 doublets, suggesting the coupling of the unpaired electron with one $I = \frac{1}{2}$ nucleus. This may be the rhodium centre (Rh, $I = \frac{1}{2}$)[36] or more likely one weakly coupled phosphorus nucleus. The values of the EPR parameters (see Table 9) are similar to those of the previous Fe^I species. Raising the temperature broadens the absorption as the intensity reduces. At the glassy-fluid transition the spectrum evolves to three isotropic signals, with relative intensities noticeably temperature dependent. Fig. 7(*b*) shows the second-derivative X-band EPR spectrum of the solution at $T = 180$ K. The g_{iso} value of the intermediate signal can be correlated to the

Table 9 X-Band EPR parameters of [Fe(triphos)(bdt)]$^-$, **2**, **3** and **6** in CH_2Cl_2 solution and the solid state[a]

Compound	g_l	g_m	g_h	$\langle g \rangle$[b]	g_{iso}	a_l	a_m	a_h	$\langle a \rangle$[b]	a_{iso}
[Fe(triphos)(bdt)]$^-$	2.093(5)	2.004(5)		2.033(5)	c	c	c	c	c	c,d
2	2.492(5)	2.018(5)	1.986(5)	2.165(5)	2.17(1)[d]	$\leqslant$30(4)[e]	28(2) 24(2)	34(2) 29(2)	$\leqslant$31(4)[e]	c,d
2 (powder)	2.442(5)	2.056(5)	2.002(5)	2.167(2)	2.08(1)[d]	c	c	c	c	c,d
3	2.190(8)	2.093(8)	1.972(8)	2.085(8)	2.139(5) (A)[f] 2.043(5) (B)[f] 2.092(5) (P)[f]	75(3)	50(5)	37(3)	54(5)	28(3)[f] 30(3)[f] 150(3)[f] 29(3)[f]
6 (A)	2.091(5)	2.007(5)	2.000(5)	2.033(5)	2.015(5)[g]	17(5)	13(5)	9(5)	13(5)	19(5)[g]
(B)	2.066(8)	1.998(8)		2.043(8)	2.061(8)[g]	265(5)	272(5)		267(5)	247(5)[g] 28(5)[g]
					2.052(5)[d]					298(3)[d] 7(3)[d]
6 (powder) (A)	2.09(1)	2.02(1)		2.04(1)	c	c	c	c	c	c

[a] T = 100 K unless otherwise stated, a values in G. [b] $\langle g \rangle = \frac{1}{3}(g_l + g_m + g_h)$ or $\frac{1}{3}(g_{\parallel} + 2g_{\perp})$; $\langle a \rangle = \frac{1}{3}(a_l + a_m + a_h)$ or $\frac{1}{3}(a_{\parallel} + 2a_{\perp})$. [c] Undetectable. [d] T = 300 K. [e] $\Delta H_i \geqslant a_i$. [f] T = 270 K. [g] T = 180 K.

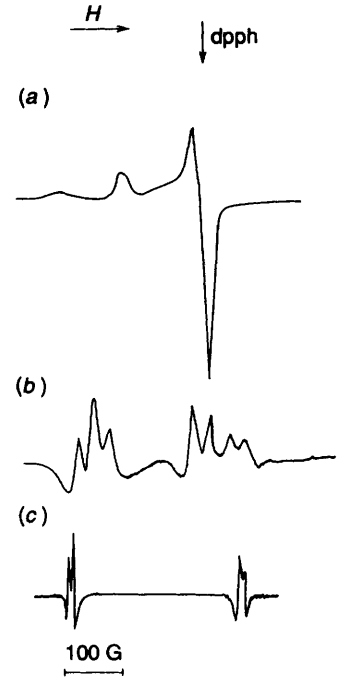

Fig. 7 X-Band EPR spectra of **6** in CH_2Cl_2 solution at T = 100 (*a*), 180 (*b*) and 300 K (*c*); (*b*) and (*c*) second derivatives

$\langle g \rangle$ of the corresponding glassy (A) species, the absorption exhibiting a partially resolved 1:1 doublet. The two outer signals constitute a second well separated doublet of broad triplets (dt). This pattern is consistent with the presence of the Rh^{II}–B species and is probably due to the coupling of the unpaired electron with two sets of magnetically non-equivalent phosphorus nuclei.[37] Higher temperatures induce drastic reduction of the central isotropic Rh^{II}–A signal while the dt pattern progressively evolves, until at T = 300 K it appears as a largely separated doublet of singlets (ds). The second derivative spectrum significantly shows a doublet of slightly separated doublets [Fig. 7(*c*)] in a lineshape dependent on the m_I(P) values.[33] This signal may be interpreted by assuming a very strong coupling of the electron with one phosphorus nucleus and, as far as the minor coupling is concerned, with the rhodium nucleus[5,34] or, alternatively, with one weakly bound phosphorus nucleus.

The spectral behaviour of the paramagnetic Rh^{II} solution appears reversible with temperature. Interestingly, decreasing the temperature to 190 K and rapidly refreezing to 100 K, the glassy lineshape is quite similar to that in Fig. 7(*a*), but it exhibits a higher spectral intensity of the anisotropic features of the Rh^{II}–B isomer. These broad signals display an axial structure ($g_{\perp} > g_{\parallel}$), with a very strong coupling with one P nucleus (Table 9). The relevant parameters compare well with the corresponding ones of the low-temperature fluid solution (dt, T = 180 K).

The X-band EPR spectrum of the microcrystalline powder of compound **6** at T = 100 K is indicative of the presence of only the isomeric Rh^{II}–A species, with the second derivative mode showing two anisotropic signals closely related to those of the glassy solution of Rh^{II}–A. The lack of superhyperfine resolution of the powder at T = 100 K is possibly due to effective electron spin–electron spin interactions between close Rh^{II} paramagnetic centres in the microcrystals, active even at very low temperature. These EPR results seem consistent with the presence of two different isomeric species of **6** in the CH_2Cl_2 fluid solution, displaying significant temperature dependence of the corresponding superhyperfine couplings and g_{iso} values. Such a temperature dependence is not surprising[38] and may support a chemical equilibrium between two rhodium(II) species of different geometry, *i.e.* one distorted towards the limiting square pyramid and one distorted towards the limiting trigonal bipyramid.[39] Fluxional behaviour of the phosphine ligand may also account for the spectral evolution of the fluid solution B isomer with temperature (*i.e.* from the dt structure to the ds one). The fluxional behaviour of phosphine–metal complexes is well known;[40] in the present study the diamagnetic derivatives **1**, **4** and **5** appear fluxional on the NMR time-scale, the phosphorus atoms of the triphos remaining equivalent up to 193 K.

References

1 I. G. Dance, *Polyhedron*, 1986, **5**, 1037; P. G. Blower and J. R. Dilworth, *Coord. Chem. Rev.*, 1987, **76**, 121; B. Krebs and G. Henkel, *Angew. Chem., Int. Ed. Engl.*, 1991, **30**, 769; M. T. Ashby, *Comments Inorg. Chem.*, 1990, **10**, 297; D. Sellmann, H. P. Neuner, M. Mall and F. Z. Knoch, *Z. Naturforsch., Teil B*, 1991, **46**, 303; A. K. Fazlur-Rahman and J. G. Verkade, *Inorg. Chem.*, 1992, **31**, 5331.

2 R. J. Angelici, *Acc. Chem. Res.*, 1988, **21**, 387.

3 J. M. Berg and R. H. Holm, in *Iron Sulfur Proteins*, ed. T. G. Spiro, Wiley, New York, 1982, vol. 4.

4 G. A. Bowmaker, P. D. W. Boyd and G. K. Campbell, *Inorg. Chem.*, 1982, **21**, 2403.

5 C. Bianchini, A. Meli, F. Laschi, A. Vacca and P. Zanello, *J. Am. Chem. Soc.*, 1988, **110**, 3913.

6 B. S. Kang, L. H. Weng, D. X. Wu, F. Wang, Z. Guo, L. R. Huang, Z. Y. Huang and H. Q. Liu, *Inorg. Chem.*, 1988, **27**, 1128.

7 C. Bianchini, A. Meli, F. Laschi, F. Vizza and P. Zanello, *Inorg. Chem.*, 1989, **28**, 227.
8 D. Sellmann, M. Geck, F. Knoch, G. Ritter and J. Dengler, *J. Am. Chem. Soc.*, 1991, **113**, 3819.
9 B. Kang, J. Peng, M. Hong, D. Wu, X. Chen, L. Weng, X. Lei and H. Liu, *J. Chem. Soc., Dalton Trans.*, 1991, 2897.
10 D. Sellmann, M. Geck, F. Knoch and M. Moll, *Inorg. Chim. Acta*, 1991, **186**, 187.
11 S. Vogel, G. Huttner and L. Zsolnai, *Z. Naturforsch., Teil B*, 1993, **48**, 641.
12 A. Togni, M. Hobi, G. Rihs, G. Rist, A. Albinati, P. Zanello, D. Zech and H. Keller, *Organometallics*, 1994, **13**, 1224.
13 P. Barbaro, C. Bianchini, F. Laschi, S. Midollini, S. Moneti, G. Scapacci and P. Zanello, *Inorg. Chem.*, 1994, **33**, 1622.
14 J. Ott, L. M. Venanzi, C. A. Ghilardi, S. Midollini and A. Orlandini, *J. Organomet. Chem.*, 1985, **291**, 89.
15 P. W. R. Corfield, R. J. Doedens and J. A. Ibers, *Inorg. Chem.*, 1967, **6**, 197.
16 N. Walker and D. Stewart, *Acta Crystallogr., Sect. A*, 1983, **39**, 158.
17 G. M. Sheldrick, SHELX 76, System of Computing Programs, University of Cambridge, Cambridge, 1976.
18 PLUTO, Cambridge Crystallographic Data Centre, University Chemical Laboratory, Cambridge, 1989.
19 *International Tables for X-Ray Crystallography*, Kynoch Press, Birmingham, 1974, vol. 4, p. 99.
20 R. F. Stewart, E. R. Davidson and W. T. Simpson, *J. Chem. Phys.*, 1965, **42**, 3175.
21 Ref. 19, p. 149.
22 J. L. Martin and J. Takats, *Inorg. Chem.*, 1975, **14**, 1358 and refs. therein.
23 H. Kopf, K. Lange and J. Pickardt, *J. Organomet. Chem.*, 1991, **420**, 345.
24 T. A. Albright, J. K. Burdett and M. Whangbo, in *Orbital Interactions in Chemistry*, Wiley, New York, 1985.
25 D. Sellmann, U. Kleine-Kleffmann, L. Zapf, G. Huttner and L. Zsolnai, *J. Organomet. Chem.*, 1984, **263**, 321.
26 M. T. Ashby, J. U. Enemark and D. L. Lichtenberger, *Inorg. Chem.*, 1988, **27**, 191.
27 M. Cowie and M. J. Bennett, *Inorg. Chem.*, 1976, **15**, 1595 and refs. therein.
28 E. R. Brown and J. R. Sandifer, in *Physical Methods of Chemistry. Electrochemical Methods*, eds. A. Weissberger and B. W. Rossiter, Wiley Interscience, New York, 1986, vol. 2.
29 C. Bianchini, F. Laschi, D. Masi, F. M. Ottaviani, A. Pastor, M. Peruzzini, P. Zanello and F. Zanobini, *J. Am. Chem. Soc.*, 1993, **115**, 2723.
30 M. C. Rakowski and D. H. Busch, *J. Am. Chem. Soc.*, 1975, **97**, 2570.
31 J. P. Lozos, B. M. Hofmann and C. G. Franz, Program No. 265, *Quantum Chemistry Program Exchange*, Northwestern University, IL, 1974.
32 F. E. Mabbs and D. Collison, in *Electron Paramagnetic Resonance of Transition Metal Compounds. Studies in Inorganic Chemistry*, Elsevier, New York, 1992, vol. 16.
33 R. Wilson and D. J. Kivelson, *J. Chem. Phys.*, 1966, **44**, 4445.
34 C. Bianchini, D. Masi, C. Mealli, G. Martini, F. Laschi and P. Zanello, *Inorg. Chem.*, 1987, **26**, 3683.
35 C. Bianchini, P. Frediani, F. Laschi, A. Meli, F. Vizza and P. Zanello, *Inorg. Chem.*, 1990, **29**, 3402.
36 G. Zotti, S. Zecchin and G. Pilloni, *J. Electroanal. Chem. Interfacial Electrochem.*, 1984, **175**, 241; G. Pilloni, G. Zotti and S. Zecchin, *J. Organomet. Chem.*, 1986, **317**, 357.
37 C. Bianchini, A. Meli, M. Peruzzini, A. Vacca, F. Laschi, P. Zanello and F. M. Ottaviani, *Organometallics*, 1990, **9**, 360; C. Bianchini, M. Peruzzini, F. Laschi and P. Zanello, in *Topics in Physical Organometallic Chemistry*, ed. M. F. Gielen, Freund, London, 1992, vol. 4.
38 C. Bianchini, D. Masi, A. Meli, M. Peruzzini and F. Zanobini, *J. Am. Chem. Soc.*, 1988, **110**, 6411; C. Bianchini, F. Laschi, M. F. Ottaviani, M. Peruzzini and P. Zanello, *Organometallics*, 1989, **8**, 893.
39 K. K. Pandey, *Coord. Chem. Rev.*, 1992, **121**, 1.
40 S. D. Ittel, P. J. Krusic and P. Meakin, *J. Am. Chem. Soc.*, 1978, **100**, 3264; D. L. DuBois and D. W. Meek, *Inorg. Chem.*, 1976, **15**, 3076; L. Dahlemburg and F. Mirzaei, *Inorg. Chim. Acta*, 1985, **97**, L1; C. A. Ghilardi, P. Innocenti, S. Midollini and A. Orlandini, *J. Chem. Soc., Dalton Trans.*, 1985, 605; F. Cecconi, P. Innocenti, S. Midollini, S. Moneti, A. Vacca and J. A. Ramirez, *J. Chem. Soc., Dalton Trans.*, 1991, 1129.

Received 21*st June* 1994; *Paper* 4/03773A